IOP Publishing Superconductor Science and Technology
Supercond. Sci. Technol. 31 (2018) 105001 (7pp) https://doi.org/10.1088/1361-6668/aad4f2

A flux-driven Josephson parametric amplifier for sub-GHz frequencies fabricated with side-wall passivated spacer junction technology

Slawomir Simbierowicz[1], Visa Vesterinen[1,2], Leif Grönberg[1], Janne Lehtinen[1], Mika Prunnila[1] and Juha Hassel[1]

[1] VTT Technical Research Centre of Finland Ltd & QTF Centre of Excellence, PO Box 1000, FI-02044 VTT, Finland
[2] QCD Labs, COMP Centre of Excellence, Department of Applied Physics, Aalto University, PO Box 13500, FI-00076 Aalto, Finland

E-mail: slawomir.simbierowicz@vtt.fi

Received 30 May 2018, revised 10 July 2018
Accepted for publication 20 July 2018
Published 24 August 2018

Abstract

We present experimental results for a Josephson parametric amplifier tailored for readout of ultra-sensitive thermal microwave detectors. In particular, we discuss the impact of fabrication details on the performance. We show that the small volume of deposited dielectric materials enabled by the side-wall passivated spacer niobium junction technology leads to robust operation across a wide range of operating temperatures up to 1.5 K. The flux-pumped amplifier has gain in excess of 20 dB in three-wave mixing and its center frequency is tunable between 540–640 MHz. At 600 MHz, the amplifier adds 105 mK ±9 mK of noise, as determined with the hot/cold source method. Phase-sensitive amplification is demonstrated with the device.

Supplementary material for this article is available online

Keywords: Josephson junction, parametric amplifier, SQUID array

(Some figures may appear in colour only in the online journal)

1. Introduction

In recent years, high-fidelity detection of radio-frequency (rf) and microwave signals that can consist of only a few photons has driven a lot of interest in the development of low-noise amplifiers. Such weak signals are encountered for instance in the search for dark matter particles [1–3], the fast readout of quantum bits (qubits) [4–7], and the characterization of low-loss resonators [8] or nano-mechanical systems [9]. A promising branch of superconducting amplifiers, with near quantum-limited noise performance, exploits parametric pumping of the non-linear inductances exhibited by Josephson junctions [10–16] or those intrinsic to superconductors [17]. The Josephson parametric amplifier (JPA) has also proven to be capable of generating and using squeezed electromagnetic states [18–20] to go below the standard quantum limit of noise added by an amplifier [21].

Although the most common applications for the JPA are in the frequency band of 4–8 GHz, we recently reported on a JPA for 600 MHz [22] to be used in conjunction with a nano-calorimeter [23, 24] or a nano-bolometer [25, 26] with a matching readout frequency. Our main motivation to develop the JPA is to allow the calorimeter to reach the accuracy of a single microwave photon and set a new record for the noise-equivalent power going below 10^{-19} W/$\sqrt{\text{Hz}}$ [27, 28] in the bolometric mode. More recently, rf reflectometry of charge qubits has also emerged as a possible use case for the sub-GHz JPA [29]. Aiming to serve such applications, the realized JPA utilized the non-linearity of niobium-based superconducting quantum interference devices (SQUIDs) in a

lumped-element rf resonator. The amplifier of [22] was narrowband, but the center frequency of the gain was designed to be tunable with an external magnetic flux. However, the device suffered from multiple issues that prohibited its immediate use in calorimetry.

The first prominent issue discovered in [22] was an unpredictable, hysteretic response of the resonance frequency to the applied magnetic flux. Its origin was attributed to flux trapping in the device geometry. The second issue was a high sensitivity to changes in the operating temperature, requiring stabilization of the JPA with closed-loop temperature control. We believe that the temperature sensitivity stemmed from two-level systems (TLSs) in a deposited dielectric layer that had a large participation ratio to the JPA resonance. This layer was made of silicon dioxide that is notorious for its high TLS density which significantly affects material properties at millikelvin temperatures [30, 31].

Here, we seek to improve on the shortcomings of [22] while keeping the design conceptually similar. We present several important modifications to the JPA, the first of which is the fabrication of the Josephson junctions with the so-called side-wall passivated spacer (SWAPS) process that we introduced recently [32]. This enables us to largely avoid using plasma-enhanced chemical vapor deposited (PECVD) silicon dioxide which is a necessity in our standard niobium tunnel junction processes [33]. Measures to control the flux trapping are implemented as well. The new JPA also employs three-wave mixing with an rf flux pump at twice the signal frequency [34] as opposed to the four-wave mixing of [22] which utilized an rf current pump [11, 13] in the vicinity of the signal frequency. We report on the measured good performance in both the non-degenerate and degenerate modes [35] of the JPA, warranting its later integration into the nano-calorimetry setup.

2. Devices

Amplifying the readout signals of a nano-calorimeter requires sufficiently high dynamic range and enough bandwidth from the JPA. More specifically, the amplifier should be able to handle input signals at a maximum power of -120 dBm without going into saturation, and it needs to respond to detector signals in the time scales of 10–1000 μs. These targets were met in [22] using a JPA realized with a lumped-element inductor–capacitor resonator for radio frequencies. The inductance originated largely from Josephson junctions in a series array of 200 SQUIDs with a maximal critical current of 35 μA. Shunted with a capacitance of $\simeq$30 pF, the flux-tunable resonator had a maximum resonance frequency f_0 of 650 MHz. The capacitive coupling to an external 50 Ω rf environment set the gain–bandwidth product to $2\pi\, f_0/Q_e \simeq 2\pi \times 2.2$ MHz, where $Q_e \simeq 300$ is the external quality factor. In this work, the device parameters are similar, and a detailed listing is provided in the supplementary information, available online at stacks.iop.org/SUST/31/105001/mmedia.

The devices (figure 1(a)) incorporate an on-chip flux bias line (FBL) on a dedicated superconductive layer. Among many solutions for FBLs [12, 13, 36–39], our implementation has the advantage that the dc bias can be routed as a twisted pair through the cryostat while the rf pump tone propagates along the same on-chip conductor. A simplified wiring schematic for the devices is shown in figure 1(b) and details are presented in the supplementary information.

The devices are fabricated with an improved process that has been reported in detail in [32]. In short, a high-resistivity silicon wafer is first cleaned of thermal oxides. Following that, the Josephson junctions of the SQUID array (figure 1(c)) are implemented with a niobium tri-layer ($Nb/Al–Al_2O_3/Nb$) with thicknesses 100 nm/10 nm/100 nm. The tri-layer is etched to a strip geometry and following the SWAPS process the sidewalls are passivated with PECVD silicon dioxide, as shown in a scanning electron micrograph in the supplementary information. Crucially, the passivation step leaves no residual dielectric layer to the device area outside the junctions. The next step is the deposition of 120 nm of niobium for the main wiring layer. The Josephson junctions form wherever this layer crosses the tri-layer strips. Because of the need for the on-chip FBL, we add a thin, 40 nm insulating layer of atomic layer deposited Al_2O_3 with wet-etched contact holes. Finally, the FBL and some superconducting crossovers are defined from 120 nm of niobium deposited as the topmost layer.

As an important detail, the capacitors of the previous JPA design [22] were formed from parallel plates separated by a silicon dioxide layer, but here we use interdigitated fingers. Our finger geometry lowers the participation ratio of the lossy, amorphous dielectrics to only 2% as confirmed by a simple electrostatic simulation [40]. In the absence of additional dielectrics, we have measured our niobium resonators to have internal quality factors of over 1×10^5 in the low-power and low-temperature limit [41]. Therefore, dielectric losses in the new amplifiers will likely arise from the remaining amorphous oxides instead of the substrate.

The initial maximum resonance frequency of the new JPAs at zero applied magnetic flux is about 500 MHz. We fine-tune it to a higher value by removing a part of the shunt capacitance with a focused ion beam (FIB) (figure 1(d)). Two nominally identical devices A and B are prepared with the maximal resonance frequency targeted at 650 MHz, in order to make flux pumping feasible at the operating frequency of 600 MHz. The chip containing the JPA is placed on a holder and inside an aluminum–Amumetal 4 K magnetic shield, both of which are thermalized to the mixing stage of a dry dilution refrigerator. Prior to parametric pumping, an initial characterization of the device takes place. It comprises the study of the small-signal response with a vector network analyzer (VNA) while tuning the resonance frequency with a magnetic flux, generated by a dc current applied to the FBL. A fit to the recorded reflection coefficient of the JPA allows us to determine the resonance frequency. Device A shows excellent reproducible tuneability between 520 MHz and 667 MHz (figure 1(e)) from which it can be concluded that the SQUID array has a relatively homogeneous magnetic flux bias. Only a slight hysteresis occurs below 640 MHz, probably in part because of the geometric inductances [42]. In contrast, the

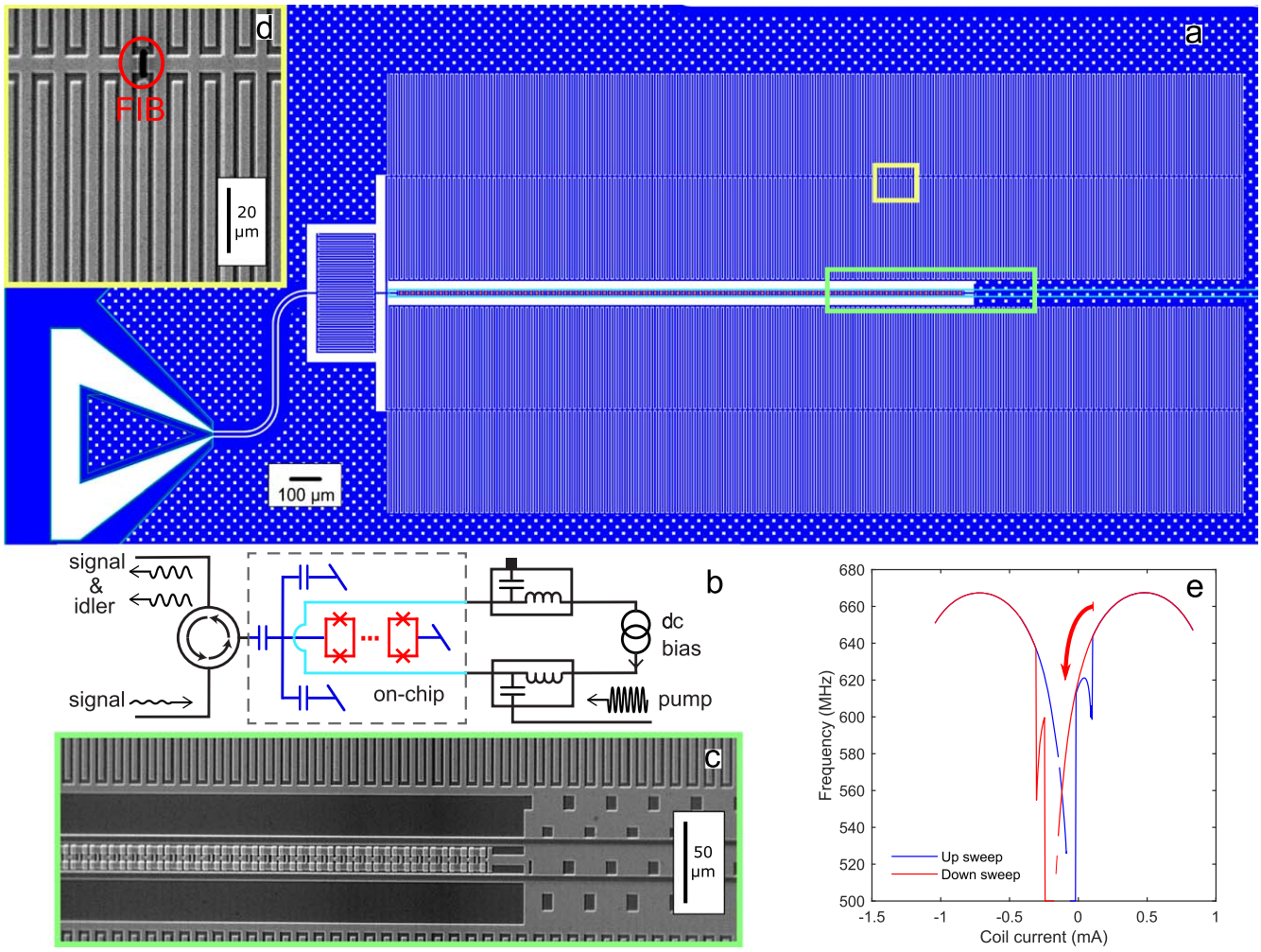

Figure 1. Layout and measurement of JPA. (a) Mask drawing showing the whole JPA with the SQUID array in red and an on-chip flux bias line (FBL) in light blue. The wiring layer in dark blue features bonding pads, shunt and coupling capacitors, and the ground plane. The holes in the ground plane trap magnetic flux. (b) Simplified measurement setup with the JPA enclosed in the dashed box. The FBL carries both a pump tone and a dc current used to bias the SQUIDs and, thus, modify the resonance frequency of the device. The probe tone enters through a circulator and three-wave mixing within the JPA allows the pump tone to produce signal and idler photons according to $f_{\mathrm{pump}} = f_{\mathrm{probe}} + f_{\mathrm{idler}}$. A second circulator (not shown) further enhances the isolation from a subsequent cascade of post-amplifiers. (c), (d) Scanning electron micrographs showing (c) a part of the SQUID array and (d) the interdigital shunt capacitor cut with a focused ion beam to fine-tune the resonance. A close-up of the other end of the array is shown in the supplementary information. (e) Tuneability of the resonance frequency of Device A. Shown are a single up sweep and a down sweep of current measured with the pump off. The arrow indicates a deterministic branch selected for subsequent measurements.

previous generation amplifier had a very irregular frequency response and only two viable operating points [22]. There are several factors that could play a role in the observed improvement. First, a ground plane with flux-trapping holes [43] has been added to the device layout. Second, we have increased the size of the SQUID loops by 65% to $2.1 \times 4.3\,\mu\mathrm{m}^2$ so that less dc current is needed in the FBL. Finally, we have paid special attention to using non-magnetic materials in close proximity to the JPA chip.

3. Gain and noise in the non-degenerate mode

The JPA operating points defined by the triplet of the dc bias current, the associated flux pump frequency, and pump power are optimized and characterized by an automated procedure described in the supplementary information. To study the gain and signal-to-noise ratio (SNR), we apply a weak probe tone at an offset of −10 kHz from the halved pump frequency where the JPA gain is maximal. The probe power is set to −146 dBm (−136 dBm) at frequencies below (above) 580 MHz, to adjust accordingly to the dynamic range. In the data of figure 2(a), the SNR is optimized at each static flux operating point, while constraining the maximum gain to 20.5 dB. A gain of 18.5–20.5 dB is attained and the SNR improves by 15–18 dB, as compared to the unity-gain reference where the noise floor is set by the high electron mobility transistor (HEMT) post-amplifier. It has been independently measured to add 10–13 K of noise. Here, the SNR and gain measurements are performed at the optimal pump power and lowering the power affects both quantities negatively, as shown in the supplementary information. As the next step, the

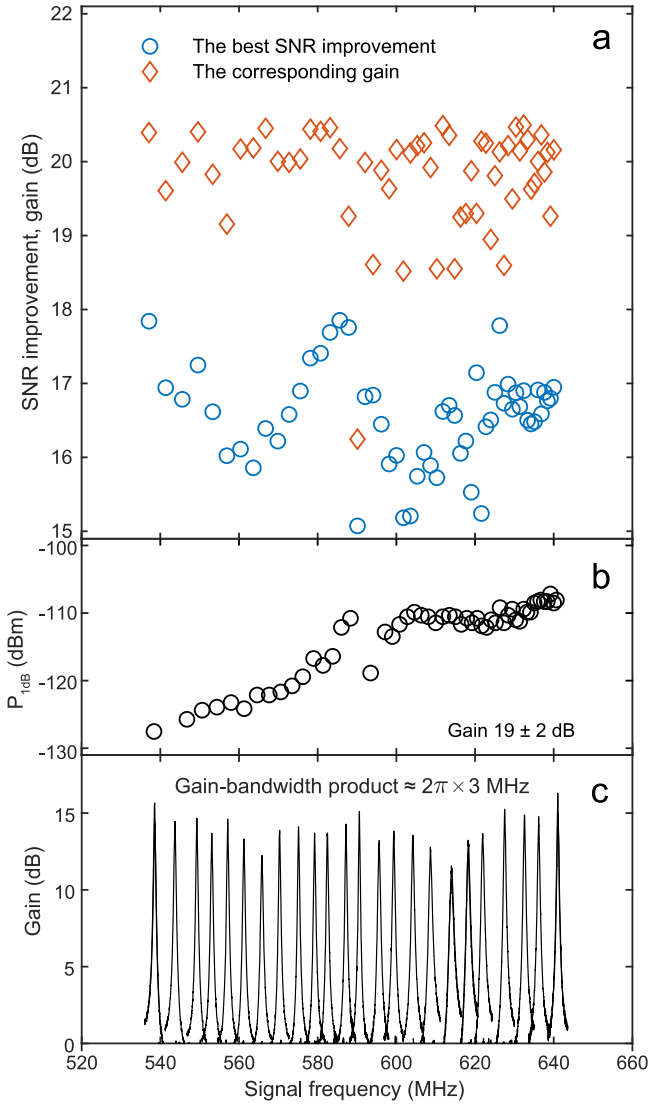

Figure 2. Systematic characterization of Device A at 10 mK. At each operating point determined by a static flux bias current, the pump power is optimized first and the gain is then adjusted with the pump frequency. The pumping fails to produce any significant gain at 590 MHz. (a) The best SNR improvement and corresponding gain while limiting to gains under 20.5 dB. The quantities are in respect to a reference that is measured with the JPA detuned and the pump switched off. (b) 1 dB compression points of gain at a probe offset of −10 kHz from the halved pump frequency where the gain is maximal. (c) Lorentzian gain profiles as a function of the signal frequency at 24 selected operating points. The target gain of each measurement was 15 dB.

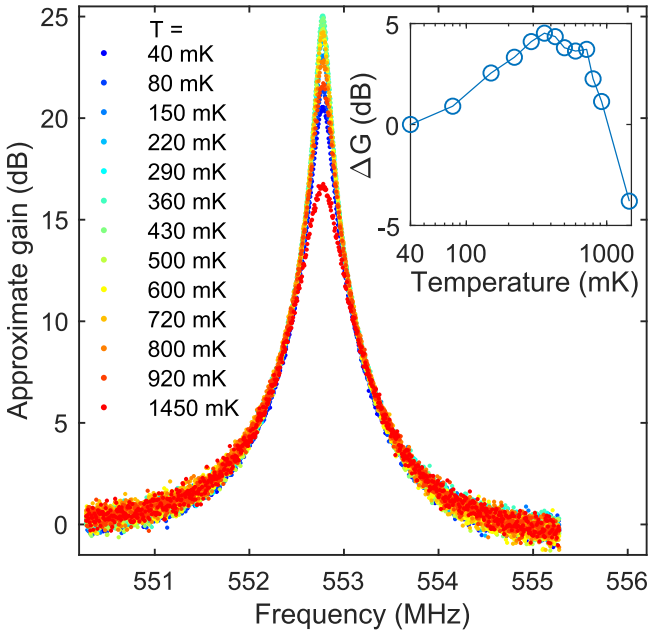

Figure 3. Approximate gain profiles for Device A at 553 MHz at varying temperatures of the sample stage starting from a gain of 20 dB at 40 mK. In the absence of reference data, the recorded signal is normalized to the edges of the peak. The pump power or frequency are not re-optimized during heating proving the temperature robustness of the amplifier. Inset: change in gain from 40 mK, as a function of temperature.

saturation of the JPA is investigated at the discovered operating points by varying the probe power (figure 2(b)) and it is found that the lower limit of −120 dBm, required for calorimeter readout, is easily surpassed by about 10 dB at 600 MHz. After increasing the pump frequency slightly to lower the gain to 15 dB, a gain–bandwidth product of $2\pi \times 3$ MHz is measured (figure 2(c)). It is sufficient for the detection of the thermal transients of the nano-calorimeter.

We investigate the potential range of the operating temperatures of Device A by setting a gain of 20 dB and measuring the JPA response with the VNA while heating the system (figure 3). The frequency and power of the flux pump are kept at the fixed values. We attribute changes in the gain to the temperature dependence of the JPA resonance frequency. Raising the temperature from 40 mK to 80 mK (400 mK) increases the gain by 1 dB (5 dB). The gain stays above 20 dB below 1.0 K, and even at 1.5 K there is still a significant 16 dB of gain. The equivalent shift of the JPA resonance is ±200 kHz, or ±0.04%. We note that these observations result from an interplay of several temperature-dependent quantities such as the permittivity of the Al_2O_3 coating of the JPA, the junction critical current, and the kinetic inductance of niobium [44].

To better estimate the noise added by the JPA, the system noise temperature is determined with the Y-factor method [45]. Essentially, the power spectral density at the output of the JPA is surveyed with a spectrum analyzer while the JPA is subject to an impedance-matched resistive noise source with a controlled temperature. The source temperature is varied between 59 mK and 852 mK independently of the JPA temperature that is held constant at 30 mK with closed-loop control. The measurements are carried out with Device B and the full setup is shown in the supplementary information. The system noise temperatures (figure 4(a)), referenced to the JPA input, are obtained from linear Y-factor fits and their uncertainties as statistical 2σ-errors. The system noise takes its minimum value of 165 mK close to the halved pump frequency. Since the noise added by the JPA is reasonably independent of the offset (figure 4(b)), we may take the average with the inverted variances as weights. This yields a noise estimate of 105 mK ± 9 mK. Making the comparison

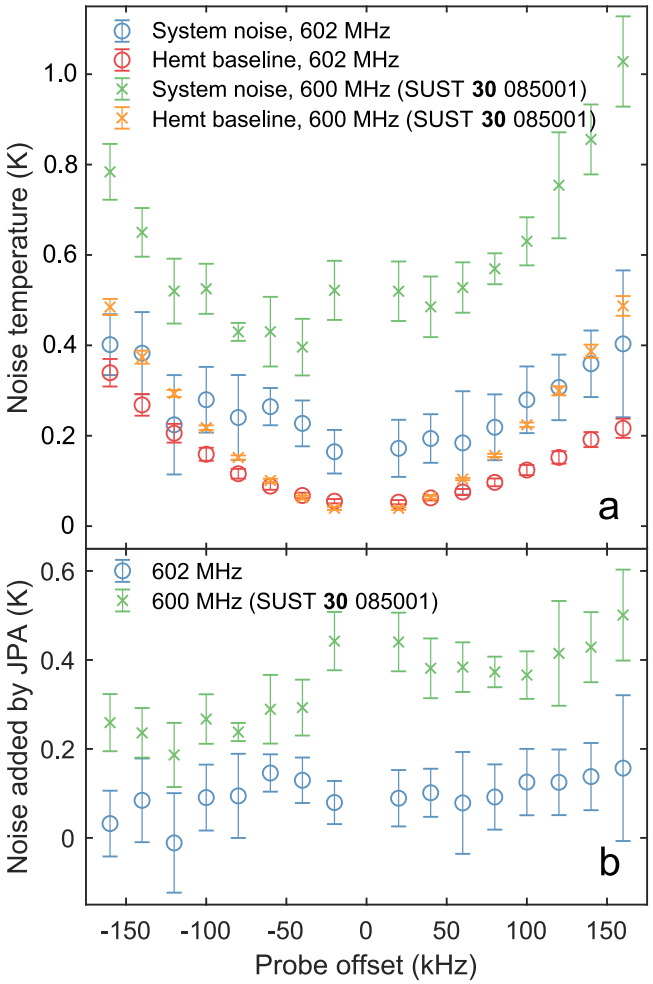

Figure 4. Noise temperature of Device B at 600 MHz determined with the Y-factor method using a calibrated noise source. Data from [22] are added for comparison. (a) System noise temperature T_{sys} as a function of the probe offset from the halved pump frequency. The separated contribution of the HEMT amplifier to T_{sys} is the smallest at zero offset where the JPA gain is maximal. (b) The noise added by the JPA is the difference between the system noise temperature and the part added by HEMT as well as the input noise: 30 mK in recent experiments and 40 mK in [22].

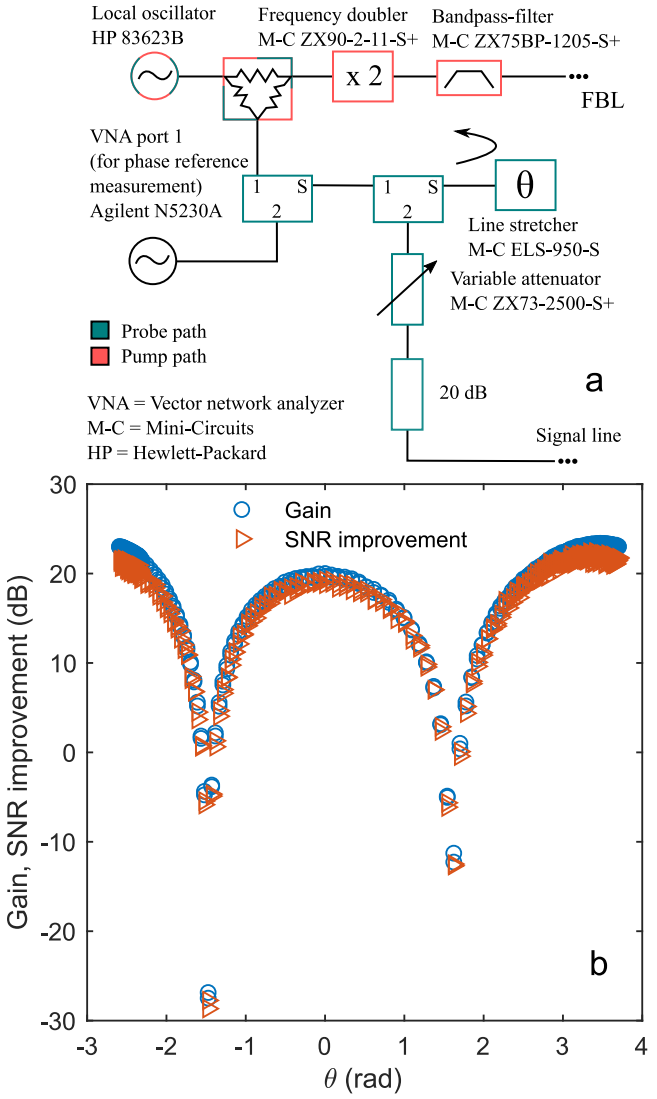

Figure 5. Device B in the degenerate mode at an operating temperature of 30 mK. The probe frequency reads $f_{\mathrm{probe}} = \frac{1}{2} f_{\mathrm{pump}} = f_{\mathrm{idler}} = 601.85$ MHz. (a) A frequency doubler generates the phase-locked pump tone. The probe is directed to a voltage-controlled electronic line stretcher (ELS) to adjust the phase difference between the probe and the pump. Afterwards, the VNA is used to calibrate the phase versus the control voltage. (b) Gain (circles) and SNR improvement (triangles) as a function of the calibrated phase. The latter is determined by comparing to a measurement where the JPA is detuned with applied magnetic flux. The observed difference of 3 dB between the gain maxima is likely caused by varying pump power, due to voltage dependence in the reflection coefficient of the ELS: a signal leaking backwards to the input of the doubler interferes with the signal following the direct path.

to [22], we note that the added noise has approximately halved. Also notable is that the noise is no longer at an elevated level at frequencies close to the gain maximum, which may be because the rf pump tone has been moved away from it to the double frequency.

4. Degenerate gain

In a dispersive sensor, such as the nano-calorimeters of [26], it is possible to choose the excitation and readout in such a way that the rf carrier and the information-carrying signal are in different quadratures. In this situation, it is possible to utilize squeezing to de-amplify the carrier and to amplify the signal. This may be used to effectively increase the dynamic range of the later stages of the readout. Ideally, the amplification does not add any noise if a JPA is used to perform the squeezing.

To observe squeezing in the degenerate mode of the JPA, where the pump is exactly at twice the probe frequency, a brief experiment is carried out with Device B. Using a single rf source, the pump is synthesized with a frequency doubler and the relative phase θ of the probe is controlled as shown in figure 5(a). The JPA gain as a function of θ is π-periodic as

expected, and amplification and de-amplification alternate. The JPA is thus capable of squeezing [46]. However, here we do not attempt a proper investigation of the quadratures to determine how much vacuum squeezing is attainable.

5. Conclusion

We have overcome all the major issues discovered with the previous generation JPA [22], and we have attained robust performance over a wide frequency range without sacrificing bandwidth, gain, or dynamic range. Additionally, we have minimized the amount of TLS-hosting dielectrics and their participation ratio with the SWAPS [32] fabrication process. This renders the JPA relatively insensitive to temperature, facilitating its use at variable mK temperatures as only minor corrections to the JPA operating parameters are needed. Furthermore, the JPA is now flux-pumped at twice the read-out frequency of the nano-calorimeter, easing the filtering required to avoid back-action such as residual heating by the pump. As an important step towards sub-GHz sensor readout at a fidelity beyond the standard quantum limit [47], squeezing has been observed in the degenerate mode of the JPA.

The noise added by the JPA has decreased to 105 mK at 600 MHz. This can largely be attributed to better isolation from the HEMT post-amplifier by means of an additional circulator. However, the added noise remains at an elevated level with respect to the lower bound set by the input thermal noise at 30 mK, likely due to poorly thermalized attenuators [48] or a fundamental limit of the amplifier itself. The noise performance also remains inferior to that of a microstrip SQUID amplifier with a reported noise temperature of 48 mK at 612 MHz [45]. However, we have demonstrated a sub-GHz JPA that is well suited for integration into a nano-calorimetry [24] or -bolometry [26] apparatus and we will pursue the latter goal in a future experiment [49].

Acknowledgments

We thank Paula Holmlund for sample preparation, Harri Pohjonen for help with lithographic masks, and Mikko Kiviranta for operating the FIB. We acknowledge the fruitful discussions with Olli-Pentti Saira, Roope Kokkoniemi, Mikko Möttönen, and Jukka Pekola. This work was performed as part of the Academy of Finland Centre of Excellence program (projects 312294, 284594, 312059, 251748, and 284621). The work also received funding from the Academy of Finland project QuMOS (project numbers 288907 and 287768), Future Makers Funding Program by Technology Industries of Finland Centennial Foundation and Jane and Aatos Erkko Foundation.

ORCID iDs

Slawomir Simbierowicz https://orcid.org/0000-0002-2435-7544
Janne Lehtinen https://orcid.org/0000-0002-5334-016X
Juha Hassel https://orcid.org/0000-0003-1002-0614

References

[1] Bradley R, Clarke J, Kinion D, Rosenberg L J, van Bibber K, Matsuki S, Mück M and Sikivie P 2003 *Rev. Mod. Phys.* **75** 777
[2] Asztalos S J *et al* 2010 *Phys. Rev. Lett.* **104** 041301
[3] Kenany S A *et al* 2017 *Nucl. Instrum. Methods Phys. Res.* A **854** 11–24
[4] Bergeal N, Schackert F, Metcalfe M, Vijay R, Manucharyan V E, Frunzio L, Prober D E, Schoelkopf R J, Girvin S M and Devoret M H 2010 *Nature* **465** 64–8
[5] Abdo B, Sliwa K, Shankar S, Hatridge M, Frunzio L, Schoelkopf R and Devoret M 2014 *Phys. Rev. Lett.* **112** 167701
[6] O'Brien K, Macklin C, Hover D, Schwartz M E, Bolkhovsky V, Zhang X, Oliver W D and Siddiqi I 2016 Towards quantum-noise limited multiplexed microwave readout of qubits *2016 IEEE MTT-S International Microwave Symposium (IMS)* pp 1–3
[7] Devoret M H and Schoelkopf R J 2013 *Science* **339** 1169–74
[8] Calusine G *et al* 2018 *Appl. Phys. Lett.* **112** 062601
[9] Clark J B, Lecocq F, Simmonds R W, Aumentado J and Teufel J D 2016 *Nat. Phys.* **12** 683–7
[10] Yurke B, Kaminsky P G, Miller R E, Whittaker E A, Smith A D, Silver A H and Simon R W 1988 *Phys. Rev. Lett.* **60** 764–7
[11] Castellanos-Beltran M A and Lehnert K W 2007 *Appl. Phys. Lett.* **91** 083509
[12] Yamamoto T, Inomata K, Watanabe M, Matsuba K, Miyazaki T, Oliver W D, Nakamura Y and Tsai J S 2008 *Appl. Phys. Lett.* **93** 042510
[13] Mutus J Y *et al* 2013 *Appl. Phys. Lett.* **103** 122602
[14] Eichler C and Wallraff A 2014 *EPJ Quantum Technol.* **1** 2
[15] Mutus J Y *et al* 2014 *Appl. Phys. Lett.* **104** 263513
[16] Eichler C, Salathe Y, Mlynek J, Schmidt S and Wallraff A 2014 *Phys. Rev. Lett.* **113** 110502
[17] Vissers M R, Erickson R P, Ku H S, Vale L, Wu X, Hilton G C and Pappas D P 2016 *Appl. Phys. Lett.* **108** 012601
[18] Mallet F, Castellanos-Beltran M A, Ku H S, Glancy S, Knill E, Irwin K D, Hilton G C, Vale L R and Lehnert K W 2011 *Phys. Rev. Lett.* **106** 220502
[19] Fedorov K G *et al* 2016 *Phys. Rev. Lett.* **117** 020502
[20] Bienfait A *et al* 2017 *Phys. Rev.* X **7** 041011
[21] Clerk A A, Devoret M H, Girvin S M, Marquardt F and Schoelkopf R J 2010 *Rev. Mod. Phys.* **82** 1155–208
[22] Vesterinen V, Saira O P, Räisänen I, Möttönen M, Grönberg L, Pekola J and Hassel J 2017 *Supercond. Sci. Technol.* **30** 085001
[23] Gasparinetti S, Viisanen K L, Saira O P, Faivre T, Arzeo M, Meschke M and Pekola J P 2015 *Phys. Rev. Appl.* **3** 014007
[24] Viisanen K L, Suomela S, Gasparinetti S, Saira O P, Ankerhold J and Pekola J P 2015 *New J. Phys.* **17** 055014
[25] Govenius J, Lake R E, Tan K Y, Pietilä V, Julin J K, Maasilta I J, Virtanen P and Möttönen M 2014 *Phys. Rev.* B **90** 064505
[26] Govenius J, Lake R E, Tan K Y and Möttönen M 2016 *Phys. Rev. Lett.* **117** 030802

[27] Karasik B S and Cantor R 2011 *Appl. Phys. Lett.* **98** 193503
[28] Suzuki T, Khosropanah P, Hijmering R A, Ridder M, Schoemans M, Hoevers H and Gao J R 2014 *IEEE Trans. Terahertz Sci. Technol.* **4** 171–8
[29] Penfold-Fitch Z V, Sfigakis F and Buitelaar M R 2017 *Phys. Rev. Appl.* **7** 054017
[30] O'Connell A D *et al* 2008 *Appl. Phys. Lett.* **92** 112903
[31] Pappas D P, Vissers M R, Wisbey D S, Kline J S and Gao J 2011 *IEEE Trans. Appl. Supercond.* **21** 871–4
[32] Grönberg L, Kiviranta M, Vesterinen V, Lehtinen J, Simbierowicz S, Luomahaara J, Prunnila M and Hassel J 2017 *Supercond. Sci. Technol.* **30** 125016
[33] Kiviranta M, Brandel O, Grönberg L, Kunert J, Linzen S, Beev N, May T and Prunnila M 2016 *IEEE Trans. Appl. Supercond.* **26** 1–5
[34] Lähteenmäki P, Paraoanu G S, Hassel J and Hakonen P J 2013 *Proc. Natl Acad. Sci.* **110** 4234–8
[35] Devoret M and Roy A 2016 *Comptes Rendus Physique* **17** 740–55
[36] Sandberg M, Wilson C M, Persson F, Bauch T, Johansson G, Shumeiko V, Duty T and Delsing P 2008 *Appl. Phys. Lett.* **92** 203501
[37] Krantz P, Reshitnyk Y, Wustmann W, Bylander J, Gustavsson S, Oliver W D, Duty T, Shumeiko V and Delsing P 2013 *New J. Phys.* **15** 105002
[38] Svensson I M, Bengtsson A, Krantz P, Bylander J, Shumeiko V and Delsing P 2017 *Phys. Rev.* B **96** 174503
[39] Zhou X, Schmitt V, Bertet P, Vion D, Wustmann W, Shumeiko V and Esteve D 2014 *Phys. Rev.* B **89** 214517
[40] Wenner J *et al* 2011 *Appl. Phys. Lett.* **99** 113513
[41] Partanen M *et al* 2018 *Sci. Rep.* **8** 6325
[42] Pogorzalek S *et al* 2017 *Phys. Rev. Appl.* **8** 024012
[43] Chiaro B *et al* 2016 *Supercond. Sci. Technol.* **29** 104006
[44] Annunziata A J, Santavicca D F, Frunzio L, Catelani G, Rooks M J, Frydman A and Prober D E 2010 *Nanotechnology* **21** 445202
[45] Kinion D and Clarke J 2011 *Appl. Phys. Lett.* **98** 202503
[46] Zhong L *et al* 2013 *New J. Phys.* **15** 125013
[47] Caves C M 1982 *Phys. Rev.* D **26** 1817–39
[48] Yeh J H, LeFebvre J, Premaratne S, Wellstood F C and Palmer B S 2017 *J. Appl. Phys.* **121** 224501
[49] Kokkoniemi R *et al* 2018 (arXiv:1806.09397)